A COMPARISON OF SCATTERING FROM 2-D AND 3-D ROUGH INTERFACE

Ningya Cheng

Earth Resources Laboratory
Department of Earth, Atmospheric, and Planetary Sciences
Massachusetts Institute of Technology
Cambridge, MA 02139

Craig A. Schultz

Lawrence Livermore National Laboratory
University of California
Livermore, CA 94550

M. Nafi Toksöz

Earth Resources Laboratory
Department of Earth, Atmospheric, and Planetary Sciences
Massachusetts Institute of Technology
Cambridge, MA 02139

ABSTRACT

In this paper we compared scattered waves from 2-D and 3-D interface structures. The modeling technique is the 3-D time domain finite difference method. The scheme is second-order accurate in time and fourth-order accurate in space. It is implemented on a massively parallel nCUBE computer. In order to investigate the characteristics of 2-D and 3-D rough surface scattering, we consider an acoustic-elastic boundary, which is described by a Gaussian autocorrelation function. The F-K analysis of reflected signals shows that 2-D scattering generates similar amounts of forward and back scattering, while in the 3-D case, more forward and less back scattering. The 3-D effects also show larger reflected energy than the 2-D case, especially near the normal incident. The out-of-plane scatterings are clearly demonstrated on the F-K spectra in the 3-D case. In the 2-D simulations, we have to keep in mind that it tends to overestimate the amount

of backscattering energy.

INTRODUCTION

Many boundaries in the Earth may be characterized as irregular interfaces, such as the ocean floor, the Moho discontinuity, and surface terrain. The wave scattering from interfaces has become a subject of wide interest. The effects of scattering on the observations can often be identified on amplitudes, traveltimes, spectra, and waveforms. Although scattering from smooth interfaces is easily modeled and well-understood, the roughness inherent in many natural interfaces introduces an incoherent component into the wavefield, which is poorly understood. A number of theoretical approaches have been developed to help us understand the rough interface scattering problem. Reviews of these works were given by Ogilvy (1987) and Thorsos and Jackson (1989). These studies are based on the perturbation method. They require interface properties, such as the overall topography (amplitude and slope), to be small compared with the incident wavelength. Under the approximation these studies give analytical solutions to the problems. Full-waveform techniques, such as the boundary integral method, are implemented to model completely the wave interaction with the interface topography (Bouchon, 1985; Kawase, 1988; Gerstoft and Schmidt, 1991; Sanchez-Sesma and Campillo, 1991). The finite difference method has also become effective in studying scattering from a rough interface (Lavender and Hill, 1985; Burns and Stephen, 1990; Dougherty and Stephen, 1991; Fricke, 1993).

Most numerical modelings have focused on two-dimensional models, such as the ocean floor, ice sheet, and shallow crust. These 2-D simulations have demonstrated the basic effects of scattering and wave conversions at interfaces. Nature boundaries, however, are three dimensional. The 3-D scattering features, such as the out-of-plane effect, cannot be addressed adequately by 2-D modeling. It is important to understand the difference between 2-D and 3-D surface scattering. This knowledge can help us assess the limitations of 2-D modeling. It is the purpose of this paper to show an example of the differences between 2-D and 3-D rough surface scattering. We chose the finite difference method as the modeling technique. The finite difference method can propagate complete wave fields through arbitrarily complex media. However, the finite difference method is very computationally intensive, especially for the 3-D problem. Parallel computing makes the finite difference method a very attractive choice. The massively parallel computer is used in this paper to implement the 3-D finite difference scheme. We chose the rough interface as an acoustic-elastic boundary. The interface is changed from 1-D (flat) to 2-D (variation in one direction) and to 3-D (variations in two directions) to do the numerical simulations. This enables us to compare the scattering from 2-D and 3-D rough surfaces directly.

3-D FINITE DIFFERENCE METHOD

Wave propagation in elastic media can be described by first-order hyperbolic equations in a Cartesian coordinate as:

$$\begin{aligned}
\rho\frac{\partial v_x}{\partial t} &= \frac{\partial \tau_{xx}}{\partial x} + \frac{\partial \tau_{xy}}{\partial y} + \frac{\partial \tau_{xz}}{\partial z} \\
\rho\frac{\partial v_y}{\partial t} &= \frac{\partial \tau_{xy}}{\partial x} + \frac{\partial \tau_{yy}}{\partial y} + \frac{\partial \tau_{yz}}{\partial z} \\
\rho\frac{\partial v_z}{\partial t} &= \frac{\partial \tau_{xz}}{\partial x} + \frac{\partial \tau_{yz}}{\partial y} + \frac{\partial \tau_{zz}}{\partial z}
\end{aligned} \tag{1}$$

and

$$\begin{aligned}
\frac{\partial \tau_{xx}}{\partial t} &= (\lambda+2\mu)\frac{\partial v_x}{\partial x} + \lambda\frac{\partial v_y}{\partial y} + \lambda\frac{\partial v_z}{\partial z} \\
\frac{\partial \tau_{yy}}{\partial t} &= \lambda\frac{\partial v_x}{\partial x} + (\lambda+2\mu)\frac{\partial v_y}{\partial y} + \lambda\frac{\partial v_z}{\partial z} \\
\frac{\partial \tau_{zz}}{\partial t} &= \lambda\frac{\partial v_x}{\partial x} + \lambda\frac{\partial v_y}{\partial y} + (\lambda+2\mu)\frac{\partial v_z}{\partial z} \\
\frac{\partial \tau_{xy}}{\partial t} &= \mu(\frac{\partial v_x}{\partial y} + \frac{\partial v_y}{\partial x}) \\
\frac{\partial \tau_{xz}}{\partial t} &= \mu(\frac{\partial v_x}{\partial z} + \frac{\partial v_z}{\partial x}) \\
\frac{\partial \tau_{yz}}{\partial t} &= \mu(\frac{\partial v_y}{\partial z} + \frac{\partial v_z}{\partial y})
\end{aligned} \tag{2}$$

where v is velocity, ρ is density, and τ is stress. λ and μ are Lamé constants. The reason for formulating the second-order wave equations into the first-order hyperbolic system of equations is that once this system is discretized on a staggered grid, it is valid for any Poisson's ratio (Virieux, 1986). The fluid-solid boundary can be treated simply by setting shear modulus to zero.

The first-order hyperbolic equations (1) and (2) are discretized on a staggered grid (Madariaga, 1976), which is shown in Figure 1. We approximate the first-order time derivative by second order centered finite difference and the first-order spatial derivatives by fourth-order centered finite difference. The media parameters ρ, λ and μ are given at the grid point where the normal stresses $\tau_{xx}, \tau_{yy}, \tau_{zz}$ are assigned (see Figure 1). In the calculation to update velocities, the needed density values are obtained from the average of the two assigned densities nearby. The shear moduli used to update the shear stress are determined by the harmonic average of the four shear moduli nearby instead of the arithmetic average (Kostek, 1991). This harmonic average method can automatically put the shear modulus zero at the fluid-solid boundary.

The dispersion analysis shows that the fourth-order finite difference has much less dispersion and grid anisotropy than the second-order one for both P and S waves. The rule of thumb is that we need five samples per wavelength for the fourth-order finite

difference to control the dispersion and the anisotropy at less than 1%. The stability condition of the scheme is given by (Cheng, 1994)

$$\Delta t < \frac{\Delta}{\sqrt{3}\alpha(|\eta_1| + |\eta_2|)} \tag{3}$$

under the condition of grid size $\Delta x = \Delta y = \Delta z = \Delta$, where $\eta_1 = \frac{9}{8}$ and $\eta_2 = -\frac{1}{24}$ are the coefficients of the fourth-order finite difference approximation to the first-order derivative. α is the maximum P wave velocity in the model. The absorbing boundary condition is applied to the outside boundaries of the grid to minimize the reflections. Higdon's absorbing boundary condition is used (Higdon, 1990).

Parallel computing provides a new means to overcome the limitations of the memory and the speed of a single processor. In the finite difference method all the calculations involve only local interactions of the velocities and stresses. For example, in the fourth-order finite difference scheme only two nearby grid points data are needed to update the current grid point. This can be efficiently executed on a multiple instruction and multiple data (MIMD) parallel computer. A staggered-grid fourth-order finite difference scheme discussed above is paralleled on nCUBE 2S massively parallel computer (Cheng, 1994).

NUMERICAL EXAMPLES AND F-K ANALYSIS

Test of the Finite Difference Method

We consider a fluid-filled cylindrical borehole embedded in a homogeneous elastic formation. The finite difference results are compared with the discrete wavenumber method. The physical property of the fluid and solid are listed in Table 1. The borehole radius is 0.1 m. A point explosion source and the pressure receivers are located at the center of the borehole. The Kelly wavelet at center frequency 14 kHz is used as the source time function (Kelly *et al.*, 1976). A grid size of 0.01 m and a time step of 0.001 ms were chosen. The second-order Higdon's absorbing boundary condition is used to reduce the artificial boundary reflections. The local P and S wave velocities are used at the absorbing boundary. A grid of $70 \times 70 \times 200$ is used to build the borehole model. The finite difference results are compared with the discrete wavenumber solutions (Cheng and Toksöz, 1981) in Figure 2. There are body waves (refracted P and S) and guided waves (Stoneley and pseudo-Rayleigh) propagated inside the borehole. The comparison shows excellent agreement between the two solutions. This test shows the finite difference scheme handled the sharp fluid-solid boundary very well. Even if the borehole is approximated by a rough edged circle in the finite difference method, we still can get a good match between the two methods.

Synthetic Reflection Data

In order to investigate the reflection characteristics from the rough surface, we consider an irregular fluid-solid interface. There are only reflected P waves in the fluid. This will greatly simplify the analysis of reflected signals. The property of the fluid and the solid are listed in Table 1 and a 3-D view of the model is shown in Figure 3. The source time function of a point explosion is a Kelly wavelet with a center frequency of 15 Hz. We choose the grid discretization interval to be one-tenth the shortest wavelength at the source center frequency, which is 100 m. The time step is 0.001 s and the size of the model is $200 \times 200 \times 100$.

In this study, we place a 2-D pressure receiver array (64×64) in a plane parallel to the interface and on one side of the source. The array receiver spacing is 20 m. We adopt a Gaussian surface to describe the fluid and solid boundary. It has a Gaussian spatial correlation function and a Gaussian distribution about the mean (Frankel and Clayton, 1986). This interface can be described by two properties: the correlation length, a, and the standard deviation in height, δ. The correlation length corresponds to the average distance between nearby peaks and valleys along the interface, and the standard deviation gives the root mean square (rms) deviation of the interface height from its mean, which is set to zero. The rms slope ϕ of the interface is given by

$$\tan(\phi) = \sqrt{2}\frac{\delta}{a} \tag{4}$$

where the correlation length is set equal to the central incident wavelength (100 m) and rms slope is set at 30 °.

A 3-D rough surface is introduced with the correlation length in the X and Y direction both equal to 100 m, while the 2-D rough interface has a correlation length in the X direction of 100 m, and of ∞ in the Y direction. The 2-D Gaussian rough surface is plotted in Figure 4a and the 3-D rough surface is plotted in Figure 4b. The 2-D rough surface is inherited from the 3-D one. It is simply obtained by extending the 3-D rough surface at Y=1 in the Y direction. This will make the amplitude comparison interesting later. In that case we obtain the amplitudes from 3-D scattering at the plane which has the exactly same surface profile as the 2-D one. The source-receiver plane is 600 m above the mean height of the rough interface.

We have calculated the synthetic data set first for a flat interface, as shown in Figure 5a. Figures 5b and c show the seismogram obtained from 2-D and 3-D rough interface models. These plots are a 2-D slice of the 3-D data set for fixed Y. The direct arrivals from the finite difference calculation are removed, and they are not shown in the plots. The coda waves in Figures 5b and c show the effect of the rough interface. The coda generated from the 2-D rough interface have more structures than the 3-D one. Also the clear reflections from the flat interface are smeared in the 2-D and 3-D rough surface cases. The F-K analysis of the reflected signals will follow.

F-K Analysis of the Reflected Data

F-K analysis is a useful technique to illustrate the magnitude and direction of energy arriving at the array. It is widely used in the seismic coda analysis, and Dainty and Toksöz (1990) give a good summary of this approach. In this case we use a simple 3-D Fourier transform algorithm on the synthetic data, transforming in both spatial directions, and in time. The data is displayed at a given frequency to show the magnitude and direction of the scattered waves. The source center frequency will be of interest here. Before we analyze the reflected data from the interfaces, we first look at the direct arrivals (Figure 6a). The direct arrivals are propagated straight from the source to the receivers on the same plane. A radius of 10 corresponds to the direct wave arriving with a horizontal phase velocity of 1.5 km/s at 15 Hz. Only half of the circle is shown on the figure. This is because the receivers are only on one side of the source. For the purpose of comparison the F-K spectra of the reflections from the flat surface is shown in Figure 6b. The small wavenumber range is because of the limited aperture of the receiver array.

Figures 6c and d give the F-K spectra for the seismograms recorded over the 2-D and 3-D interfaces. The F-K spectra for the 2-D interface clearly shows that similar amounts of both backscattered and forward scattered energy are present in the seismogram. This distribution is in agreement with the numerical mean reflection coefficients presented for the 2-D interface by Schultz and Toksöz (1993a), which show similar amounts of both forward and back scattering. The structure of the spectra is parallel to the K_y just like the rough surface is parallel to the Y axis. The F-K spectra for the 3-D interface also shows a large amount of both forward and back scattered energy. However, the forward scattered energy appears to be dominant. This suggests that more forward scattering appears to exist. However, one must remember that it is possible for energy, which is diffracted back towards the seismic line from a side scatterer, to appear with a positive K_x wavenumber. Thus, in the 3-D case, out-of-plane scattering can give the appearance of more forward scattering and less backscattering. Nevertheless, these results appear to support the results of Schultz and Toksöz (1993b), which showed, based on experimental data, that 3-D interfaces tend to show a more rapid decrease in backscattering combined with a more rapid increase in forward scattering as an incident wave arrives at larger incident angles (with respect to the vertical). In the 3-D case the wide spread of energy in the F-K spectra clearly demonstrates the out-of-plane reflections.

Figure 7 gives the rms amplitude of the primary reflection versus incident angle. The seismogram section is taken from Y=1, where the 3-D and the 2-D surface have the same profile. The geometric spreading is compensated according to the flat interface. The rms amplitudes of the first cycle is shown in Figure 7a. The 2-D and 3-D rms amplitudes are similar, but they are both smaller than the flat interface amplitude. This is exactly what we expected. As we add more cycles into the rms amplitude (Figure 7b), more scattered energy is accounted for. It clearly shows that the extra degree of freedom associated with the 3-D interface geometry can result in a larger contribution of scattered energy. The 3-D variation of the interface topography results

in a larger amplitude than the 2-D one near normally incident angles. This gives a first estimate of the scaling differences between the 2-D and 3-D reflection coefficients studied by Schultz (1994) in his thesis, where the rms amplitude from 2-D numerical calculations and 3-D ultrasonic experiments are compared. The out-of-plane contributions from 3-D topography also result in the amplitude being larger than the flat interface.

SUMMARY

The 3-D time domain finite difference method is used to investigate the rough fluid-solid interface scattering. The scheme is implemented on the nCUBE 2S massively parallel computer. The synthetic reflection data is analyzed by the F-K spectra. The 2-D scattering clearly shows the similar amount of forward and backward scattering, while in the 3-D case out-of-plane reflections give more forward scattering and less back scattering. The 3-D effects are also shown on the larger reflected rms amplitude than the 2-D case near normally incident angles. This is because of the contributions from out-of-plane scattering from 3-D topography. This 3-D out-of-plane scattering can be easily identified on the F-K spectra.

In this paper we only take a first step to demonstrate the difference of 2-D and 3-D surface scattering. More thorough investigations are needed. For example, we need to test a large amount of realizations of the interface to obtain statistical insight into 2-D and 3-D rough surface scattering. In our simulation we only consider the point source. To achieve high angular resolution of the reflection, we need to form a beam to the interface instead of the point source (Stephen and Swift, 1994). This will give us a more quantitative measure of the 2-D and 3-D reflection.

ACKNOWLEDGMENTS

This research was supported by the ERL/nCUBE Geophysical Center for Parallel Processing at M.I.T. and by Air Force Office of Scientific Research contract #F49620-94-1-0282.

REFERENCES

Bouchon, M., 1985, A simple, complete numerical solution to the problem of diffraction of SH waves by an irregular surface, *J. Acoust. Soc. Am. 77.* 1–5.

Burns, D.R. and Stephen, R.A., 1990, Three-dimensional numerical modeling of geoacoustic scattering from seafloor topography, *J. Acoust. Soc. Am., 88,* 2338–2345

Cheng, N., 1994, Borehole wave propagation in isotropic and anisotropic media: 3-D finite difference approach, *Ph.D. Thesis*, Massachusetts Institute of Technology, Cambridge, MA.

Cheng, C.H. and Toksöz, M.N., 1981, Elastic wave propagation in a fluid-filled borehole and synthetic acoustic logs, *Geophysics, 46,* 1042–1053.

Dainty, A.M. and Toksöz, M.N., 1990, Array analysis of seismic scattering, *Bull. Seis. Soc. Am., 80,* 2242–2260.

Dougherty, M.E. and Stephen, R.A., 1991, Seismo/acoustic propagation through rough seafloors *J. Acoust. Soc. Am., 90.* 2637–2651.

Frankel, A. and Clayton, R., 1986, Finite difference simulations of seismic scattering: Implications for the propagation of short-period seismic waves in the crust and models of crustal heterogeneity, *J. Geophys. Res., 91,* 6465–6489.

Fricke, J.R., 1993, Acoustic scattering from elemental arctic ice features: Numerical modeling results, *J. Acoust. Soc. Am., 93,* 1784–1796.

Gerstoft, P. and Schmidt, H., 1991, A boundary element approach to ocean seismoacoustic facet reverberation, *J. Acoust. Soc. Am., 89,* 1629–1642.

Higdon, R.L., 1990, Radiation boundary conditions for elastic wave propagation, *SIAM J. Numer. Anal., 27,* 831–870.

Kawase, H., 1988, Time-domain response of a semi-circular canyon for incident SV, P and Rayleigh waves calculated by the discrete wavenumber boundary element method, *Bull. Seis. Soc. Am., 78,* 1415–1437.

Kelly, K.R., Ward, R.W., Treitel, S., and Alford, R.M., 1976, Synthetic seismograms: A finite-difference approach, *Geophysics, 41,* 2–27.

Kostek, S., 1991, Modelling of elastic wave propagation in a fluid-filled borehole excited by a piezoelectric transducer, *Masters Thesis*, Massachusetts Institute of Technology, Cambridge, MA.

Lavender, A.R. and Hill, N.R., 1985, P-SV resonances in irregular low velocity surface layers, *Bull. Seism. Soc. Am., 75,* 847–864.

Madariaga, R., 1976, Dynamics of an expanding circular fault, *Bull. Seism. Soc. Am., 65,* 163–182.

Ogilvy, J.A., 1987, Wave scattering from rough surfaces, *Rep. Prog. Phys., 50,* 1553–1608.

Sanchez-Sesma, F.J. and Campillo, M., 1991, Diffraction of P, SV and Rayleigh waves by topographical features: A boundary integral formulation, *Bull. Seis. Soc. Am., 81.* 2234–2253.

Schultz, C.A., 1994, Enhanced backscattering of seismic waves from irregular interfaces, *Ph.D. Thesis*, Massachusetts Institute of Technology, Cambridge, MA.

Schultz, C.A. and Toksöz, M.N., 1993a, Enhanced backscattering of seismic waves from a highly irregular, random interface: SH case, *Geophys. J. Int., 114.* 91–102.

Schultz, C.A. and Toksöz, M.N., 1993b, Enhanced backscattering of seismic waves from a highly irregular, random interface: P-SV case, *Geophys. J. Int., 117.* 783–810.

Stephen, R.A. and Swift, S.A., 1994, Modeling seafloor geoacoustic interaction with a numerical scattering chamber, *J. Acous. Soc. Am., 96,* 973–990.

Thorsos, E.I. and Jackson, D.R., 1989, The validity of the perturbation approximation for rough surface scattering using a Gaussian roughness spectrum, *J. Acous. Soc. Am., 86,* 261–277.

Virieux, J., 1986, P-SV wave propagation in heterogeneous media: Velocity-stress finite difference method, *Geophysics, 51,* 889–901.

	P wave velocity α (m/s)	S wave velocity β (m/s)	density ρ (g/c.c.)
Fluid	1500	—	1.0
Solid	4000	2300	2.3

Table 1: The velocity and the density values of the fluid and the solid.

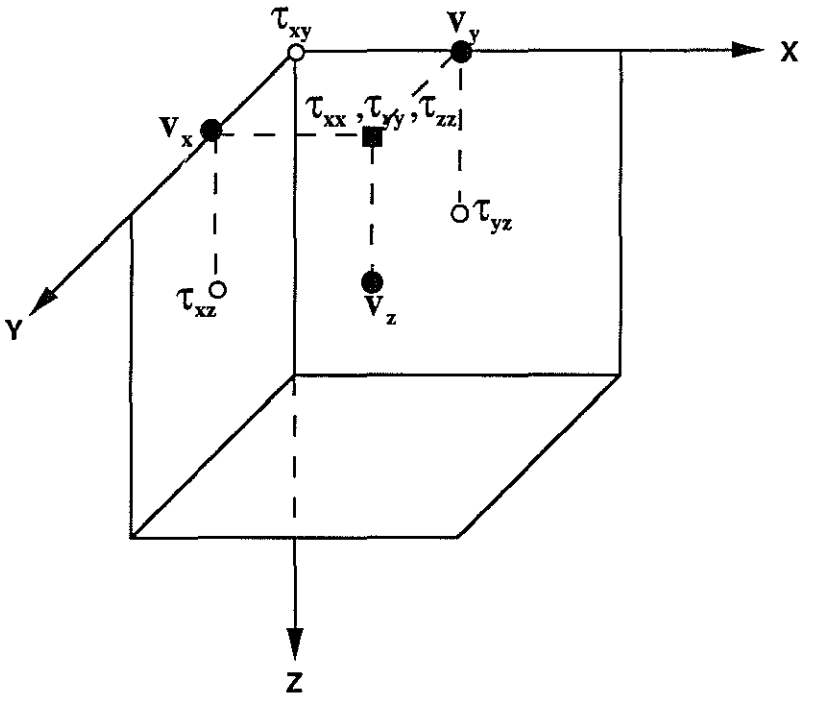

Figure 1: Staggered grid used to discretize equations (2.5) and (2.6). Solid circles represent the velocities. Open circles represent the shear stresses. The solid square represents the normal stresses.

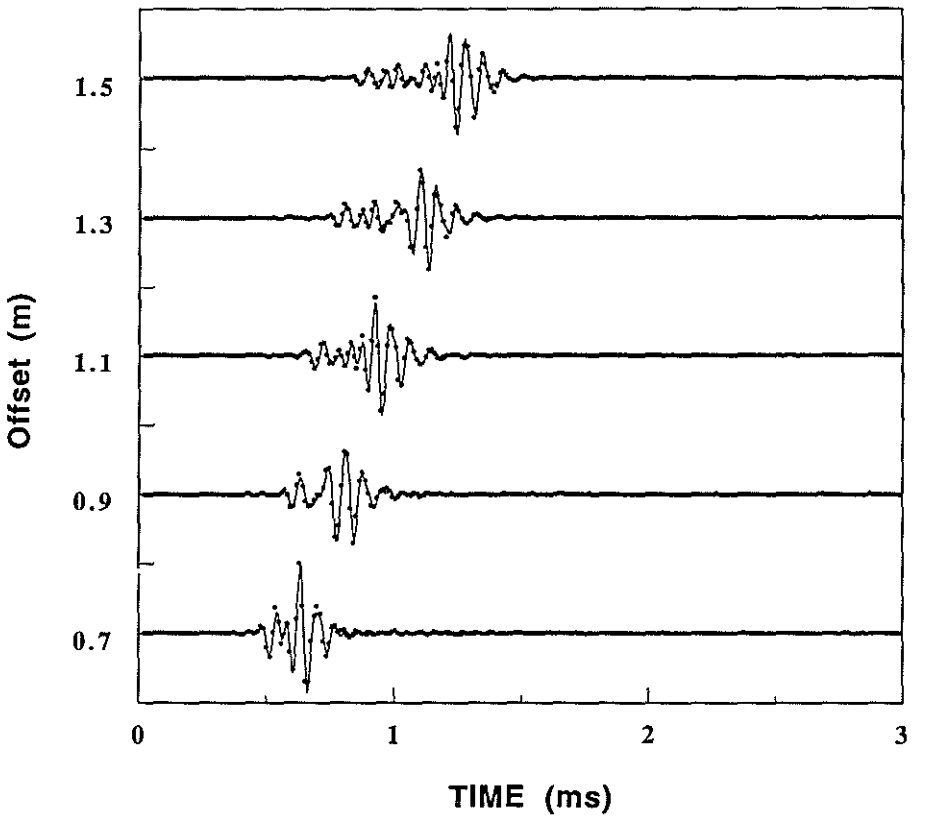

Figure 2: Comparison of the finite difference solutions (solid line) with the discrete wavenumber solutions (dot) in a fluid-filled borehole. The explosion source at center frequency 14 kHz is used. The amplitudes are normalized.

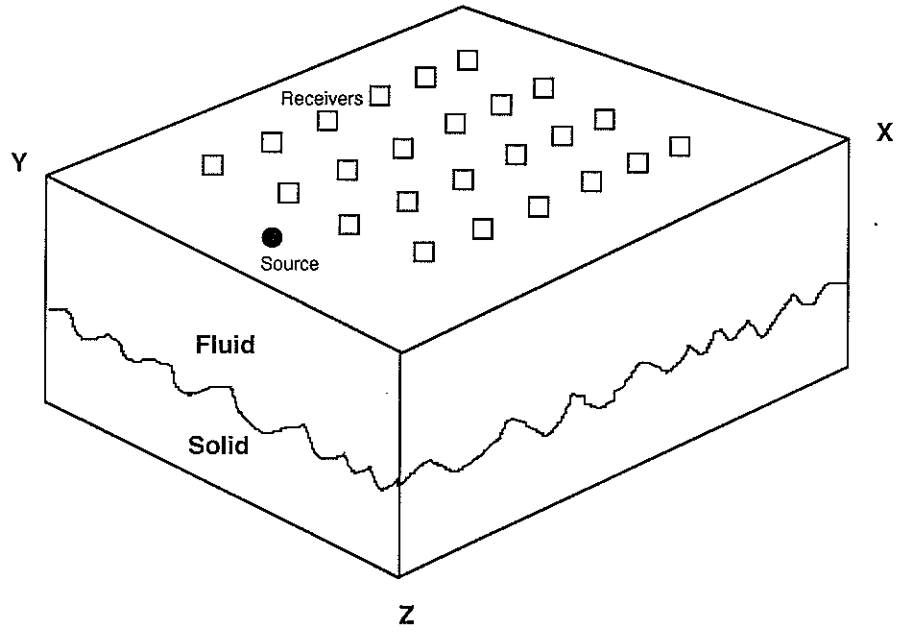

Figure 3: Schematic diagram of the model geometry used to compute the synthetic rough interface reflection data. The source-receiver arrangement is also shown.

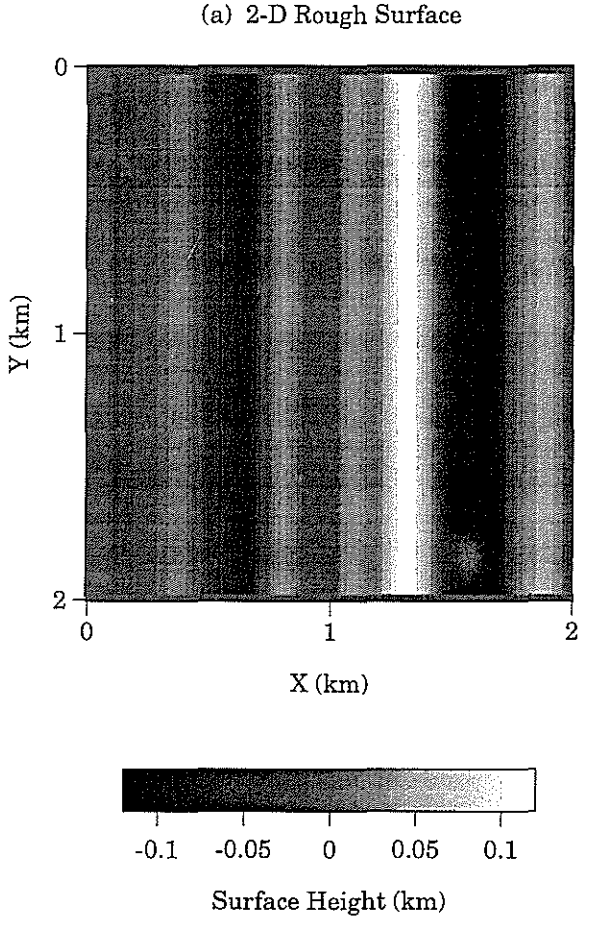

Figure 4: One example of a Gaussian rough surface. The correlation length is 100 m and the rms slope is 30 degrees. (a) 2-D rough interface, (b) 3-D rough interface.

(b) 3-D Rough Surface

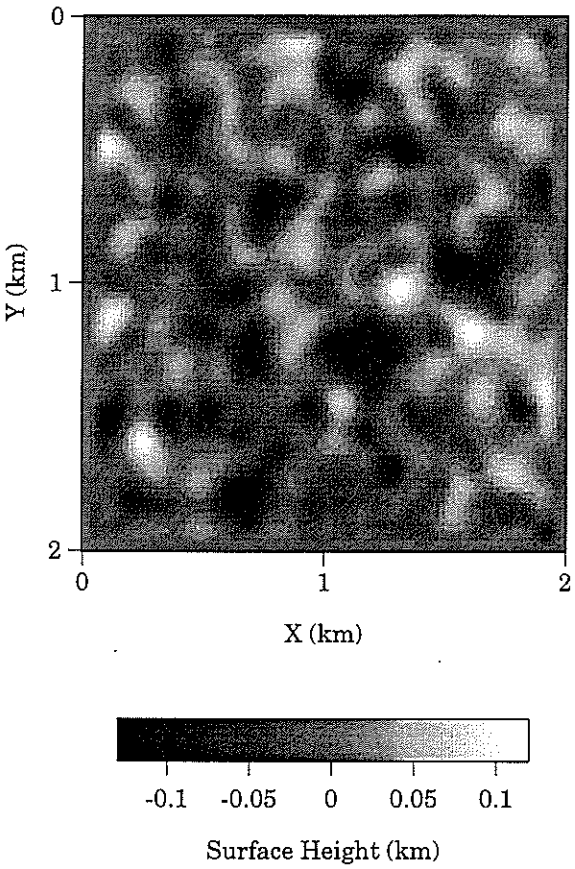

Figure 4: continued

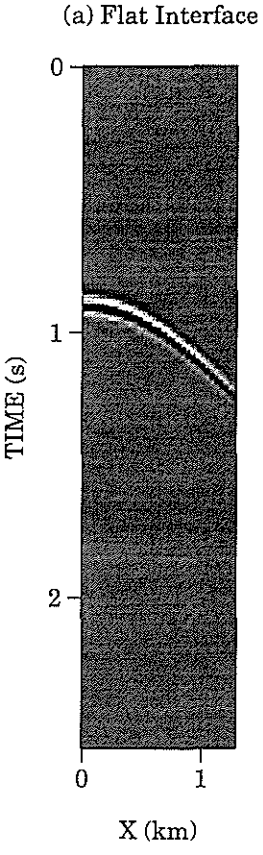

Figure 5: Synthetic seismograms of fluid-solid interface reflections. They are 2-D slices of the 3-D data set. The direct arrivals are removed from the data set. (a) flat interface, (b) 2-D rough interface, (c) 3-D rough interface.

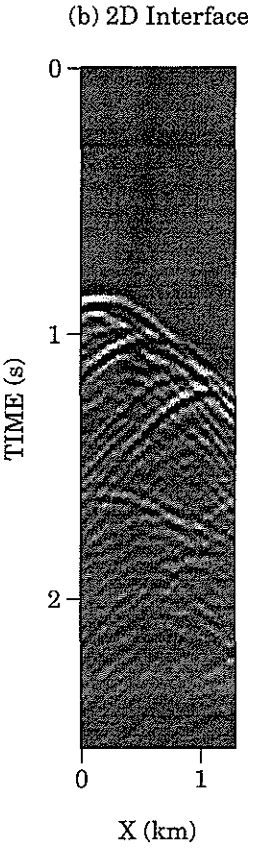

Figure 5: continued

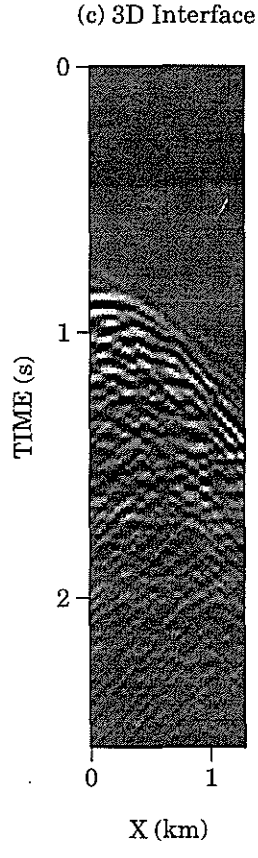

Figure 5: continued

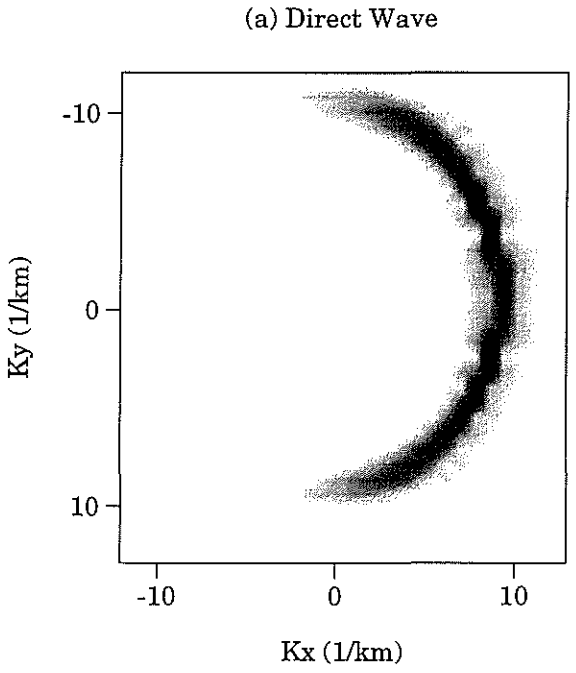

Figure 6: FK plots of synthetic data at frequency 15 Hz. (a) direct arrivals, (b) flat interface reflection, (c) 2-D rough interface reflection, (d) 3-D rough interface reflection.

(b) Flat Interface

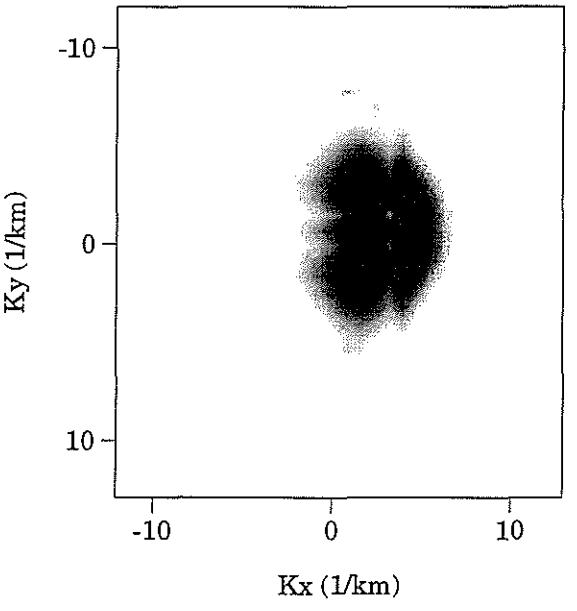

Figure 6: continued

(c) 2D Interface

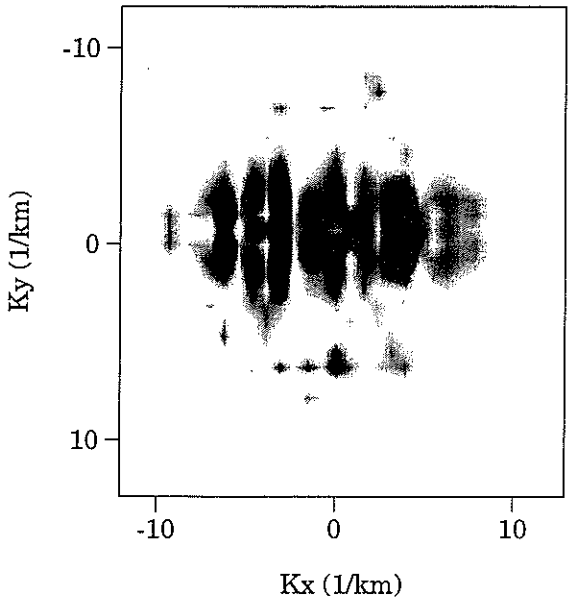

Figure 6: continued

(d) 3D Interface

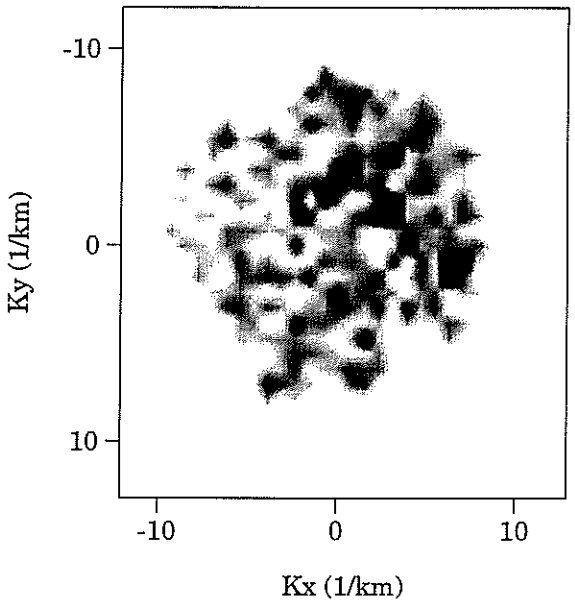

Figure 6: continued

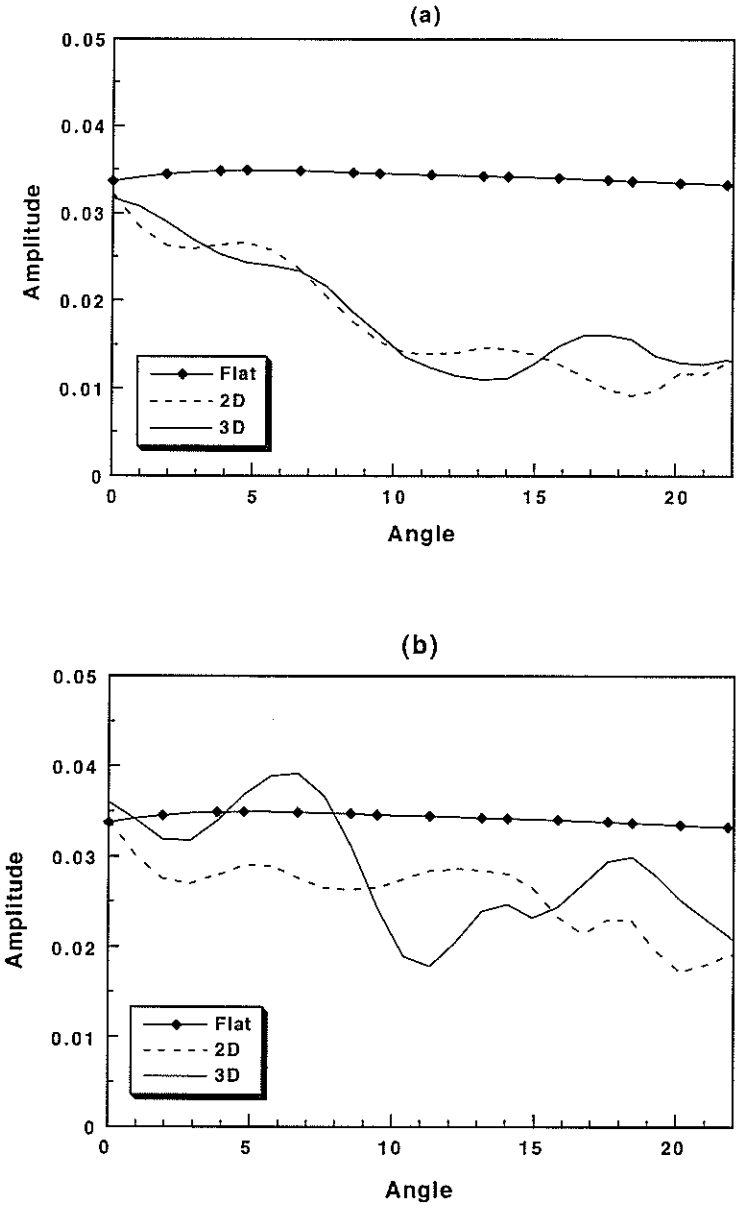

Figure 7: Plot illustrating the rms amplitudes of the waves reflected from the flat, 2–D and 3–D interfaces. Amplitude scale is arbitrary. (a) first cycle of the primary reflection, (b) first 2 cycles of the primary reflection.